DTIC FILE COPY

AD-A214 502

PORT DOCUMENTATION PAGE

1a. RESTRICTIVE MARKINGS	
2a. SECURITY CLASSIFICATION	3. DISTRIBUTION/AVAILABILITY OF REPORT: Approved for public release, distribution unlimited
2b. DECLASSIFICATION/DOWNGRADING SCHEDULE	
4. PERFORMING ORGANIZATION REPORT NUMBER(S): N/A	5. MONITORING ORGANIZATION REPORT NUMBER(S): AFOSR-TR- 89-1324
6a. NAME OF PERFORMING ORGANIZATION: The Regents of the University of California	6b. OFFICE SYMBOL (If applicable):
7a. NAME OF MONITORING ORGANIZAT ON: Air Force Office of Scientific Research (AFSC) Bolling Air Force Base, DC 20332-6448	
6c. ADDRESS (City, State and ZIP Code): University of California, San Diego La Jolla, CA 92093	7b. ADDRESS (City, State and ZIP Code): Air Force Office of Scientific Research (AFSC) Bolling Air Force Base, DC 20332-6448
8a. NAME OF FUNDING/SPONSORING ORGANIZATION: Dept. of the Air Force	8b. OFFICE SYMBOL (If applicable): NE
9. PROCUREMENT INSTRUMENT IDENTIFICATION NUMBER: AFOSR-85-0371	
8c. ADDRESS (City, State and ZIP Code): Air Force Office of Scientific Research (AFSC) Bolling Air Force Base, DC 20332-6448	10. SOURCE OF FUNDING NOS.

PROGRAM ELEMENT NO.	PROJECT NO.	TASK NO.	WORK UNIT NO.
61102F	2305	B1	

11. TITLE (Include Security Classification): Hybrid (Optical/Electronic) Computing & Digital Optical Computing

12. PERSONAL AUTHOR(S): Lee, Sing H.

13a. TYPE OF REPORT	13b. TIME COVERED	14. DATE OF REPORT (Yr., Mo., Day)	15. PAGE COUNT
Final Technical	FROM 9/1/85 TO 8/31/88		

16. SUPPLEMENTARY NOTATION

17. COSATI CODES			18. SUBJECT TERMS (Continue on reverse if necessary and identify by block number)
FIELD	GROUP	SUB. GR.	

19. ABSTRACT (Continue on reverse if necessary and identify by block number)

SEE ATTACHMENT

DTIC ELECTE NOV 20 1989 S B D

20. DISTRIBUTION/AVAILABILITY OF ABSTRACT: UNCLASSIFIED/UNLIMITED ☒ SAME AS RPT. ☐ DTIC USERS ☐	21. ABSTRACT SECURITY CLASSIFICATION: UNCLASSIFIED
22a. NAME OF RESPONSIBLE INDIVIDUAL: Dr. Lee Giles/Dr. Alan Craig	22b. TELEPHONE NUMBER (Include Area Code): (202)767-4931
	22c. OFFICE SYMBOL: NE

DD FORM 1473, 83 APR EDITION OF 1 JAN 73 IS OBSOLETE.

SECURITY CLASSIFICATION OF THIS PAGE

89 11 17 074

ABSTRACT

The AFOSR program at UCSD contains mainly two areas of optical information processing research:

(i) Optical-analog/electronic hybrid computing

In hybrid optical-analog/electronic computing, we have performed several new studies for optical image processing, optical pattern recognition and optical solution of partial differential equations. For example, in image processing we designed and fabricated space variant filters to optically implement numerous space-variant transformations (e.g., Hough transform for detection of high-order parametric curves, coordinate transforms to detect rotation and scale invariant features of images, etc.). For spike removal from noisy images, we have developed a new parallel algorithm suitable for optical-analog/electronic hybrid implementation. This parallel algorithm is space-variant and performs better than the space-invariant low-pass filter and the time-consuming median filter. We also studied a single beam interferometer, with a special photorefractive $BaTiO_3$ crystal, which effectively subtracts an exponentially weighted history of the input from the current value, thus functioning as a time-differentiating (or novelty) filter. The single beam interferometer uses signal beam depletion from photorefractive amplification of noise (fanout) in a specially designed and cut $BaTiO_3$ photorefractive crystal (with input faces cut parallel to (100), (011) and $(01\bar{1})$ crystallographic planes).

For optical pattern recognition we have completed the comparison study of statistical pattern recognition algorithms by investigating the performances of their discriminant filters when implemented by phase only (PO) filters. We found that for each of the pattern recognition algorithms studied (e.g., least-square linear mapping technique (LSLMT) simplified LSLMT (SLSLMT), Hotelling Trace Criterion (HTC), Foley-Sammon (FS) transform, and Fukunaga-Koontz (FK) transform) the peak of the correlation intensity increases and the size of the correlation spot decreases when a PO filter is used. The signal-to-noise ratio was improved for the LSLMT, SLSLMT and the FK filters, but deteriorated for the HTC and the FS filters. Continuing our search for new, more robust optical pattern recognition algorithms, we have formulated a nonlinear transformation based on minimization of a special energy function, (i.e., self-organization neural network). In contrast to these supervised learning algorithms based on data of known statistics, this unsupervised learning algorithm does not require *a priori* knowledge of the statistics of the input data. To implement the nonlinear transformation for optical pattern recognition we are constructing a hybrid optical/electronic system based on random-phase coded matrix-tensor multiplier, which can provide in parallel and in real time a large number (e.g. $\sim 10^6 - 10^9$) of adaptive optical connections and therefore allow operation on large size images.

For the optical solution of partial differential equations by a confocal Fabry-Perot system with optical feedback and photorefractive gain, we have shown that the analog accuracy of the optical solutions to partial differential equations can be improved by implementing an iterative error correcting algorithm.

(ii) Digital optical computing and nonlinear optical devices:

In digital optical computing research, ~~we have been~~ developing nonlinear optical devices and studying their uses in parallel architectures for implementation of parallel algorithms. The nonlinear optical devices are based on integrating silicon with PLZT. ~~Using~~ LPCVD techniques to deposit polycrystalline Si onto the electro-optic PLZT substrate and then recrystallizing the polysilicon using an Ar^+ laser to produce single crystal silicon grains, ~~we have~~ fabricated and tested a 12 × 12 electrically addressed spatial light modulator (SLM) array and a 16 × 16 optically addressed SLM array.

To study optical parallel computing architectures, we investigated different interconnection topologies and have generated holographic optical elements to implement fully interconnected and hypercube interconnected topologies.

FINAL TECHNICAL REPORT

ON

HYBRID (OPTICAL/ELECTRONIC) COMPUTING AND DIGITAL OPTICAL COMPUTING

for

Air Force Office of Scientific Research
(AFOSR-85-0371)

by

Sing H. Lee
Department of Electrical Engineering and Computer Sciences
University of California, San Diego
La Jolla, CA 92093

October 2, 1989

Table of Contents

1. Introduction

The AFOSR program at UCSD consists of two areas of optical information processing: (i) optical-analog/electronic hybrid computing for optical image processing, optical pattern recognition and solution of partial differential equations, and (ii) nonlinear optical devices and digital optical computing. The optical-analog/electronic digital hybrid system consists of an analog optical processor with input/output interfaces to a microcomputer. The analog optical processor is employed to perform time consuming computations, while the logical decisions and controls are provided by an electronic microcomputer. For image processing we have implemented, with hybrid systems, numerous space-variant transformations (e.g., Hough transforms for detection of high-order parametric curves, coordinate transforms for rotation and scale invariant feature extraction, etc.). For spike removal from noisy images we have developed a new parallel algorithm for optical implementation, whose performance is superior to that of low-pass or median filters. For motion detection, image clutter removal and novelty filtering we have constructed and experimentally evaluated a time-differentiating (or novelty) filter, which consists of a single beam interferometer based on a specially designed $BaTiO_3$ photorefractive crystal (with input faces cut parallel to (100), (011) and $(01\bar{1})$ crystallographic planes). For optical statistical pattern recognition we studied the implementation of discriminant functions of our phase-coded processor using phase only filters. We also formulated a new nonlinear transform for unsupervised optical pattern recognition, which is presently being implemented by a hybrid optical/electronic system based on a random-phase coded matrix-tensor multiplier. Finally, for the optical solution of partial differential equations with the hybrid system based on a confocal Fabry-Perot processor, we have shown that the analog accuracy of the optical solutions can be improved by implementing an iterative error correcting algorithm.

In the digital optical computing research, we have been developing nonlinear optical devices and studying their uses in parallel architectures for implementations parallel algorithms. Nonlinear optical devices based on integrating silicon with PLZT were fabricated and tested (e.g., a 12×12 electrically addressed spatial light modulator and a 16×16 optically addressed spatial light modulator). In our attempt to construct digital optical processing systems we have fabricated optical holograms for implementation of architectures of fully and hypercube interconnection topology. Now, we are investigating the replacement of optical holograms by computer generated holograms for programmable optical interconnects and volume holograms in photorefractive crystals for reprogrammable optical interconnects.

2. Hybrid (Optical-Analog/Electronic Micro-) Computer

2.1. Optical Image Processing

2.1.1. Optical space-variant filters for image transformations

In the study of digital image processing algorithms, which would benefit from optical implementation, we have constructed a computerized optical system for design and generation of space-variant holographic filters (see Fig. 1) [1]. Employing this system, space-variant filters containing 256 × 256 sub-holograms have been generated in 649F and dichromatic gelatin plates for optical Hough transforms of high-order parametric curves and for coordinate transforms. These filters have been used in the real time space-variant optical/electronic processor of Fig. 2 to detect the three parameters of a circle and the four parameters of an ellipse; the experimental performance is summarized in Fig. 3 and Fig. 4 respectively. Furthermore, to perform rotation and scale invariant image transformation, we have generated a $\ell n\, r - \theta$ coordinate transform filter for images of size 256 × 256 pixels. The experimental results on performance of this filter are shown in Fig. 5 and Fig. 6. Details can be found in Ref. 1.

2.1.2. Parallel optical algorithm for image spike noise removal

We have developed a new parallel algorithm for image spike noise removal suitable for optical processing implementation. The new algorithm is space-variant and performs better than the simple space-invariant low-pass filter used to reduce noise in low-level image processing, (see Figure 7(b)), and the time-consuming median filter (see Figure 7(c)). The space-variant algorithm for spike noise removal can be applied to a large size image and is based on comparing the intensity of a pixel $I(i,j)$ with the average intensity of its nearest neighbors $(\bar{I}(i,j))$. If $|I(i,j)-\bar{I}(i,j)|$ is greater than the local variance of the nearest neighbors, then we replace $I(i,j)$ by $\bar{I}(i,j)$, otherwise the original value of $I(i,j)$ is preserved. Computer simulation results (see Figure 7(d)) show that the proposed algorithm removes spike noise without blurring the image. Table I summarizes quantitatively the performance of the proposed algorithm and compares it with the conventionally used spike noise removal algorithms (i.e., median and low pass filter).

2.1.3. Optical time-differentiating filter for image motion analysis

We have demonstrated a single beam interferometer which effectively subtracts an exponentially weighted history of the input from the current value, thus functioning as a novelty filter [2]. The filter uses signal depletion from photorefractive amplification of noise (fanout). Input which is stationary for longer than the photorefractive response time is strongly depleted, but any portions of the input which change their phase, amplitude, wavelength or polarization are immediately transmitted. The gain material used was a crystal of photorefractive barium titanate with its surfaces on the (1,0,0), (0,1,1) and $(0,1,\bar{1})$ crystallographic planes, so that the

optic axis lies at 45 degrees to the input face, allowing access to the peak gain with normal signal incidence [3]. This crystal provided higher gain and faster response than the normally cut material. To examine the time-differentiating filter's real time operation, we used a hybrid optical/electronic system with input/output interfaces: a liquid crystal light valve is used to convert a video image into a phase and/or amplitude modulated input signal and a CCD camera is used as an optical to electronic converter. The experimental results are shown in Fig. 8. A contrast ratio of 100 was observed between moving and stationary images, with a resolution limited only by that of the light valve. Potential applications of this filter include image clutter removal, motion detection and analysis, tracking, edge enhancement, and image time differentiation.

2.2. Optical Pattern Recognition

2.2.1. Comparative Study of Phase Only Filter for Statistical Pattern Recognition

We have recently completed a study of phase-only-filtering applied to discriminant functions provided by various statistical pattern recognition algorithms. Phase-only (PO) filtering employs only the phase of the filtering function while the amplitude is set equal to 1 at all points on the filter. We performed computer simulations in order to evaluate the effect of PO filtering as compared to amplitude and phase (AP) filtering. The performances of PO and AP filtering were evaluated using the following characteristics: peak correlation intensity, correlation spot size, signal-to-noise ratio and optical efficiency. We were interested in measuring these characteristics for the discriminant functions provided by various statistical pattern recognition algorithms that have been under investigation at UCSD. The five different algorithms we evaluated in conjunction with the PO filtering study were: the Least Squares Linear Mapping Technique (LSLMT) [4], the Simplified Least Squares Linear Mapping Technique (SLSLMT) [5], the Hotelling Trace Criterion (HTC) [6], the Foley-Sammon Transform (FS) [7] and the Fukunaga Koontz transform (FK) [8]. The training and test data we used consisted of grey tone images of 64×64 pixels with one byte of grey tone data per pixel. Our training set was composed of 5 such images of tanks and 5 of trucks. Our test data set was composed of 4 tank and 4 truck images.

For each algorithm we created two filters (i.e., PO and AP) using the two classes of training images. The test images were then used to compute the various evaluation characteristics. The simulation results are summarized in Tables 2-6 for evaluation of LSLMT, SLSLMT, HTC, FS and FK transforms. The results obtained indicate that for all algorithms the peak correlation intensity increases and the correlation spot size decreases when a PO filter is used. The signal-to-noise ratio improved for the LSLMT, SLSLMT and the FK filters but deteriorated for the HTC and the FS filters. The optical efficiency did not show a significant change in either direction.

2.2.2. Nonlinear Transformations for Pattern Recognition

The feature extraction process of a pattern recognition system can be considered as a function f that maps a set of input patterns $\underline{x}$ onto a set of features $f(\underline{x})$. The criteria usually used for designing the feature extraction function is to minimize an error energy function E, which is defined as $\|f(\underline{x})-\Gamma(\underline{x})\|^2$, where $\Gamma(\underline{x})$ is the desired output feature.

Conventional pattern recognition systems [4-9] use pre-designed and fixed linear filters f, which are implemented based on *a priori* knowledge of the input patterns. If an adaptive pattern recognition system is desired, the function f is implemented with a recursive algorithm [10-12], where an on-line learning rule is enforced to adjust f successively. Usually the function $\Gamma(\underline{x})$ is determined by the statistics of the input pattern. Therefore, for data of known probability density function, $\Gamma(\underline{x})$ can be considered given and the adaptive process can be seen as supervised learning. However, those systems will not work well in a changing environment, where the statistics of the input patterns are usually not predictable, or do not obey the simplified gaussian assumption. Furthermore, for some complicated patterns, due to nonlinear characteristics, patterns may not be well classified by the most frequently used linear discriminant function in the feature domain. Therefore, nonlinear transformations or nonlinear feature extraction processes should be employed to extract more effective features in order to gain higher accuracy and reliability in pattern classification.

We have already shown that an adaptive pattern recognition system may be put in terms of neural network systems as an adaptive hetero-associative memory [12]. The learning process of a hetero-associative memory is equivalent to the supervised on-line training of an adaptive pattern recognition system, while recalling information from a hetero-associative memory is equivalent to the feature extraction process of an adaptive pattern recognition system. Both the adaption rule of a pattern recognition system and the learning rule of a hetero-associative memory are methods that minimize the errors between the actual outputs and the desired outputs.

To overcome the problems of conventional pattern recognition systems as stated above, we have been developing a neural network which utilizes the concept of self-organization [11,13,14] to optimize the solution without having input statistics. The proposed neural network is based on the minimization of a special energy function, $E' \equiv \|f_2(f_1(\underline{x}))-\underline{x}\|^2$, where both f_1 and f_2 are, in general, nonlinear. In fact, the energy function is a mean-square difference (error) between the true pattern $\underline{x}$ and the estimate pattern $\hat{\underline{x}} = f_2(f_1(\underline{x}))$. Without knowing any input statistics, the network will self-organize its interconnections by adaptively modifying their strength in a direction that minimizes the energy function E'. This energy minimization process will result in optimum transformations f_1 and f_2, so that the resultant self-organizing feature vector $f_1(\underline{x})$ will optimally describe the input data statistics. This is different from the self-organization algorithm developed from the gradient method [11,13] and the algorithm based on cooperative-competitive learning [14].

The energy minimization process for self-organization will require the development of techniques capable of finding the desired optimum nonlinear transformations f_1 and f_2. In supervised learning one of the widely used techniques is the delta rule [9]. We are studying the extension of the delta rule as applied to the minimization of the energy function E' for unsupervised learning. Another technique used in unsupervised learning is the simulated annealing algorithm which is, in fact, a stochastic approach. The simulated annealing algorithm is well suited for the minimization of the proposed energy function, and therefore is also under investigation.

To implement the discussed algorithm optically we are presently constructing an optical neural network architecture based on a real time random phase coded matrix-tensor multiplier interfaced to a microcomputer. This optical memory (see Fig. 9) will be capable of storing a very large number of optical connections ($\sim 10^6 - 10^9$) using a photorefractive crystal. All these connections can be accessed in parallel and in real time to provide the output matrix for electronic thresholding and calculation of a correction term for the tensor according to the learning rule. The correction term will be used to update the optical interconnection stored in the photorefractive memory material.

2.3. Solution of Partial Differential Equations

The Bimodal Error Reduction (BER) algorithm is used for improving the accuracy of the solutions obtained from a moderate-accuracy processor [15,16]. Our investigation involves the experimental application of this algorithm to satisfy the desired accuracy requirements on an electronic/optical hybrid processor being constructed. The optical portion of this hybrid processor performs the analog solution of Poisson's equation for a two-dimensional input image. The electronic portion updates the input image and performs support functions. We have theoretically analyzed the error correction algorithm applied to Poisson's operator, which led to an expression for the condition of convergence. Also, a computer simulation of the hybrid (electronic/optical) implementation of the algorithm was performed to confirm the theoretical analysis. The theoretical development considered additive error on the operator in the analog processor and on the input image presented to the analog processor. Both error functions were assumed to be spatially and temporally constant in this development. Conditions for convergence of the algorithm under these assumptions were determined and found to include the expected operating conditions of the hybrid (analog/digital) processor being constructed.

A simulation of the BER algorithm as implemented on the hybrid processor confirmed the theoretical results (see Table 7). Refinement of the solution to 8-bit accuracy is obtained in four iterations. Next we enhanced the computer simulation to more realistically represent the characteristics of the hybrid processor. For example, Table 8 shows the results obtained when using a sinusoidal (i.e., multi-grey level) input image and a sinusoidal error function for the operator. Again convergence of the algorithm is obtained. In particular, we see achievement of better than 8-bit accuracy in the final solution after only four error correcting iterations.

3. Nonlinear Optical Devices and Digital Optical Computing

3.1. Si/PLZT Opto-Electronic Devices for DOP

Using low pressure chemical vapor deposition (LPCVD) techniques to deposit polycrystalline Si onto the electro-optic PLZT substrate and then recrystallize the polysilicon using an Ar^+ laser to produce single crystal silicon grains, we have fabricated a 12 × 12 electrically-addressed spatial light modulator (SLM) array and a 16 × 16 optically-addressed SLM array [17]. The schematic diagrams of the electronic circuits for the two devices are shown in Fig. 10.

Each pixel of the ESLM array consists of a driving transistor, a reset line and the E-O modulator. An electrical input drives the NMOS transistor, the output of which in turn controls the modulator. In experiments performed in the last year, we have achieved excellent transistor performance characteristics which are shown in Fig. 11 [18]. Figure 11a shows the I-V characteristics of the NMOS transistor and Fig. 11b shows the time response characteristics of the ESLM. We have achieved breakdown voltages of 48V which is at least a factor of 2 greater than that of previously reported thin film transistors [19]. The transconductance was $200\mu s$ which then yielded a calculated value of 550 cm^2/Vs for the mobility. We are at present in the process of measuring the storage time, the leakage current and the optical modulation depth of these modulator arrays.

The performance characteristics of the OSLM array are shown in Fig. 12. In this device we have demonstrated the fabrication of a CMOS device on an electro-optic substrate. Breakdown voltages of 28v were achieved for the NMOSFET. The transconductance was $100\mu s/V$ and the mobility was 442 cm^2/Vs [19]. The major improvement of the performance characteristics resulted from the optimization of the process steps and the improved crystal grain growth obtained using laser recrystallization.

3.2. Digital Optical Processing

To study optical parallel computing architectures, we investigated different interconnection topologies and have generated holographic optical elements (HOEs) that implement (a) fully interconnected and (b) hypercube interconnected topologies [20]. These HOEs were space-variant holograms designed and generated by the computerized system of Fig. 1, and were recorded in dichromatic gelatin to provide diffraction efficiency of better than 80%. Reconstructions from one sub-hologram (PE) for fully connected and one for a hypercube interconnected architecture are shown in Figs. 13 and 14, respectively. Recently, we are investigating the replacement of optical holograms by computer generated holograms for programmable optical interconnects and volume holograms in photorefractive crystals for reprogrammable optical interconnects.

4. List of Publications in the Past Twelve Months

4.1. Journal Publications

1. Z. H. Gu, Sing H. Lee and Y. Fainman, "Statistical recognition of color images," *Appl. Opt.*, **26,** 3145-3152, (1987).
2. Q. Tian, Y. Fainman, Z. H. Gu and Sing H. Lee, "Comparison of statistical pattern recognition algorithms for hybrid processing. Part I: Linear mapping algorithms," *J. Opt. Soc. Am.*, A5(10):1655-1669 (October 1988).
3. Q. Tian, Y. Fainman and Sing H. Lee, "Comparison of statistical pattern recognition algorithms for hybrid processing. Part II: Eigenvector-based algorithms," *J. Opt. Soc. Am.*, A5:1670-1682 (October 1988).
4. H. Farhoosh, Y. Fainman and S. H. Lee, "Algorithm for computation of large size FFTs in computer generated holograms by interlaced sampling," *Opt. Eng.* **28** (6):622-628 (June 1989).
5. K. Urquhart, S. H. Lee, C. Guest, M. Feldman, and H. Farhoosh, "Computer aided design of computer generated holograms for electron beam fabrication" *Appl. Opt.* **28** (15):3387-3395 (August 15, 1989).
6. P. Ambs, Y. Fainman, S. H. Lee and J. Gresser, "Computerized design and generation of space-variant holographic filters: Part 1: System design considerations and applications of space-variant filters to image processing," *Appl. Opt.*, 27 (22):4753-4760 (November 15, 1988).
7. P. Ambs, Y. Fainman, S. Esener and S. H. Lee, "Computerized design and generation of space-variant holographic filters: Part 2: Applications of space-variant filters to optical computing," *Appl. Opt.*, **27** (22):4761-4755 (November 15, 1988).
8. J. Jau, Y. Fainman and S. H. Lee, "Comparison of artificial neural networks with pattern recognition and image processing" *Appl. Opt.*, **28** (2):302-305 (January 15, 1989).
9. J. Ford, Y. Fainman and S. H. Lee, "Time integrating interferometry using photorefractive fanout," *Opt. Lett.*, **13** (10):856-858 (October 1988).
10. Y. Fainman and S. H. Lee, "Advances in applying nonlinear optical crystals to optical signal processing," ch. 12, ed. by C. H. Chen, *Handbook of Signal Processing*, pp. 349-377, Marcel Dekker, Inc., (1988).
11. H. Farhoosh, M. R. Feldman, S. H. Lee, C. C. Guest, Y. Fainman and R. Eschbach, "A comparative study of encoding schemes for E-beam fabrication of computer generated holograms," *Appl. Opt.*, **26** :4361-4372, (October 1987).
12. H. Farhoosh, Y. Fainman, S. H. Lee, "Algorithm for computation of large size Fourier transforms in computer-generated holograms by interlaced sampling." *Opt. Eng.* **28** (6): 622-628 (June 1989).

4.2. Presentation and Conference Proceedings

1. J. H. Wang, T. H. Lin, S. C. Esener, S. Dasgupta and S. H. Lee, "NMOS transistors fabricated by simultaneous laser assisted crystallization and diffusion on silicon on electrooptic PLZT," *Proc. of Mat. Res. Soc. Symposium,* Boston, Massachusetts (November 1987).
2. P. Ambs, Y. Fainman, S. H. Lee and J. Gresser, "Computerized design and generation of space-variant holographic filters," presented at the *SPIE Conference on Optoelectronics and Laser Applications in Science and Engineering," Los Angeles, January 1988.*
3. P. Ambs, Y. Fainman, S. Esener and S. H. Lee, "Holographic optical elements for SLM defect removal and for optical interconnect," presented at the *SPIE Conference on Optoelectronics and Laser Applications in Science and Engineering,* Los Angeles, January 1988.
4. R. Eschbach, H. Farhoosh, Y. Fainman and S. H. Lee, "An algorithm for computation of large size FFTs in computer generated holograms by interlaced sampling," presented at the *SPIE Conference on Optoelectronics and Laser Applications in Science and Engineering,* Los Angeles, January 1988.
5. C. C. Guest, M. Feldman, R. Eschbach, Y. Fainman and Sing H. Lee, "Design of computer generated holograms for electron beam fabrication by means of a computer aided design system," presented at the *SPIE Conference on Optoelectronics and Laser Applications in Science and Engineering,* Los Angeles, January 1988.
6. J. H. Wang, S. C. Esener, T. H. Lin, S. Dasgupta and S. H. Lee, "Two dimensional electrically addressed Si/PLZT spatial light modulator arrays," presented at the *Topical Meeting on Spatial Light Modulators and Applications,* June 15-17, 1988, Lake Tahoe, Nevada.
7. T. H. Lin, J. H. Wang, S. Dasgupta, S. C. Esener and S. H. Lee, "A 1D optically addressed silicon/PLZT spatial light modulator array," presented at the *Topical Meeting on Spatial Light Modulators and Applications,* June 15-17, 1988, Lake Tahoe, Nevada.
8. J. E. Ford, Y. Fainman and Sing H. Lee, "Improved photorefractive performance from a special cut of $BaTiO_3$" presented at the *Topical Meeting on Spatial Light Modulators and Applications,* June 15-17, Lake Tahoe, Nevada.
9. Q. Tian, Y. Fainman and S. H. Lee, "Comparison of eigenvector-based statistical pattern recognition algorithms for hybrid processing," presented at the *SPIE International Symposium on Optical Engineering and Industrial Sensing,* June 1988.

5. References

1. P. Ambs, Y. Fainman, S. H. Lee and J. Gresser, "Computerized design and generation of space-variant holographic filter," *Appl. Opt.* **27** (22):4753-4760 (November 15, 1988).
2. J. Ford, Y. Fainman and S. H. Lee, "Time integrating interferometry using photorefractive fan out," *Opt. Lett.* **13** (10):856-858 (October 1988).
3. J. Ford, Y. Fainman and S. H. Lee, "Improved photorefractive performance from a special cut of $BaTiO_3$, *Topical Meeting on Spatial Light Modulators and Applications, Technical Digest,* Lake Tahoe, Nevada 1988.
4. Z.-H. Gu, J. R. Leger and S. H. Lee, "Optical implementation of the least-square linear mapping technique for image classification," *J. Opt. Soc. Am.*, **72** (6):787-793 (June 1982).
5. Z. H. Gu and S. H. Lee, "Recognition of images of Markov-1 model by least-squares linear mapping technique, *Appl. Opt.*, **23** :822-827 (1984).
6. Z. H. Gu and S. H. Lee, "Optical implementation of the Hotelling trace criterion for image classification," *Opt. Eng.* **23** :727-731 (1984).
7. Q. Tian, M. Barbero, Z. H. Gu and S. H. Lee, "Image classification by Foley-Sammon transform, *Opt. Eng.* **25** :834-840 (1986).
8. J. R. Leger and S. H. Lee, "Image classification by an optical implementation of the Fukunaga-Koontz transformation," *J. Opt. Soc. Am.*, **72** (5):556-564 (May 1982).
9. Q. Tian, Y. Fainman, Z. H. Gu and S. H. Lee, "Comparison of statistical pattern recognition algorithms for hybrid processing: Part I and Part II, *J. Opt. Soc. Am.*, **A5** :1655-1682 (October 1988).
10. A. D. Fisher and C. L. Giles, "Optical adaptive associative computer architectures," *Proc. IEEE COMPCON* 342-344 (Spring 1985).
11. T. Kohonen, *Self-Organization and Associative Memory,* Springer-Verlag, 1983, Chapter 7.
12. J. Y. Jau, Y. Fainman and S. H. Lee, "Comparison of artificial neural networks with pattern recognition and image processing," *Appl. Opt.* **28** (2):302-305 (January 15, 1989).
13. R. Hecht-Nielson, "Counter-propagation network neurocomputer," private communication.
14. G. A. Carpenter and S. Grossberg, "Associative learning, adaptive pattern recognition and cooperative-competitive decision making by neural network," *SPIE,* **654:** 128-247 (1986).
15. J. H. Wilkinson, *Rounding Errors in Algebraic Processes,* 121-134 (Prentice-Hall, Englewood Cliffs, NJ, 1964),
16. H. J. Caulfield, J. H. Gruninger, J. E. Ludman, K. Steiglitz, H. Rabitz, J. Gelfanc and E. Tsoni, "Bimodal optical computers," *Appl. Opt.* **25,** 3128 (Sept. 15, 1986).
17. S. H. Lee, S. Esener, M. Title and T. Drabik, "Two-dimensional silicon/PLZT spatial light modulators: design considerations and technology," *Opt. Eng.* **25** (2):250-260, (February 1986).

18. J. H. Wang, S. C. Esener, T. H. Lin, S. Dasgupta and S. H. Lee, "Two dimensional electrically addressed Si/PLZT spatial light modulator arrays," presented at the *Topical Meeting on Spatial Light Modulators and Applications,* June 15-17, 1988, Lake Tahoe, Nevada; A manuscript has been submitted to *Appl. Opt.* (1989).

19. T. H. Lin, J. H. Wang, S. Dasgupta, S. C. Esener and S. H. Lee, "A two-dimensional optically addressed silicon/PLZT spatial light modulator array," presented at the *Topical Meeting on Spatial Light Modulators and Applications,* June 15-17, 1988, Lake Tahoe, Nevada; A manuscript has been submitted to *Appl. Opt.* (1989).

20. P. Ambs, Y. Fainman, S. Esener and S. H. Lee, "Holographic optical element for SLM defect removal and for optical interconnects," *Appl. Opt.* **27** (22):4761-4755 (November 15,1988).

Table 1.

This table shows the mean square error of estimate image for three different spike removal algorithms and seven different noise levels. It is clearly shown that the performance of the space-variant filter is much better than the others, especially, for the very noisy image.

spike removal algorithms	number of spike pixels in a 256 × 256 image						
	100	500	1000	2000	3000	4000	50000
low-pass filter - median filter	90.72 - 66.15	111.51 - 70.04	143.87 - 76.68	201.89 - 80.49	272.39 - 86.77	356.39 - 95.68	447.27 - 104.53
space-variant filter	59.48	62.18	66.44	67.20	68.94	73.31	77.55

Table 2. Comparative Correlation Results

	Amplitude and Phase (standard) LSLMT filter				Phase-only LSLMT filter			
Input	Peak correlation intensity	Area of correlation spot	I_p/N_{rms}	η_h	Peak correlation intensity	Area of correlation spot	I_p/N_{rms}	η_h
Tank vs. tank filter	1.67×10^{-2}	943	4.78	1.72×10^{-2}	1.10×10^{-2}	72	12.75	1.53×10^{-2}
Tank vs. truck filter	8.75×10^{-7}	8385	2.69×10^{-4}	3.91×10^{-2}	5.78×10^{-2}	25	7.74	3.38×10^{-3}
Truck vs. tank filter	3.11×10^{-7}	7800	1.09×10^{-4}	3.2×10^{-4}	5.94×10^{-2}	56	7.13	1.93×10^{-2}
Truck vs. truck filter	3.60×10^{-2}	63	11.45	6.03×10^{-3}	1.90×10^{-1}	64	20.70	4.50×10^{-2}

Table 3. Comparative Correlation Results

	Amplitude and Phase (standard) SLSLMT filter				Phase-only SLSLMT filter			
Input	Peak correlation intensity	Area of correlation spot	I_p/N_{rms}	η_h	Peak correlation intensity	Area of correlation spot	I_p/N_{rms}	η_h
Tank vs. tank filter	1.45×10^{-2}	1196	4.33	1.7×10^{-2}	8.47×10^{-2}	30	9.38	9.68×10^{-3}
Tank vs. truck filter	4.75×10^{-3}	285	1.36	6.13×10^{-3}	3.44×10^{-2}	25	4.84	3.47×10^{-3}
Truck vs. tank filter	7.72×10^{-4}	2756	0.26	1.22×10^{-2}	0.175	42	21.20	2.20×10^{-2}
Truck vs. truck filter	4.40×10^{-2}	90	11.795	9.25×10^{-3}	0.228	42	34.71	4.76×10^{-2}

Table 4. Comparative Correlation Results

	Amplitude and Phase (standard) HTCfilter				Phase-only HTC filter			
Input	Peak correlation intensity	Area of correlation spot	I_p/N_{rms}	η_h	Peak correlation intensity	Area of correlation spot	I_p/N_{rms}	η_h
Tank vs. tank filter	1.035	1855	194.6	6.05×10^{-3}	1.565	399	142.0	1.77×10^{-2}
Tank vs. truck filter	0.73	2268	142.8	1.24×10^{-2}	1.36	216	91.0	1.15×10^{-2}
Truck vs. tank filter	0.66	1240	172.6	2.92×10^{-3}	1.37	391	121.1	1.85×10^{-2}
Truck vs. truck filter	0.76	518	196.4	2.54×10^{-3}	2.22	176	146.2	8.98×10^{-3}

Table 5. Comparative Correlation Results

	Amplitude and Phase (standard) FSN filter				Phase-only FSN filter			
Input	Peak correlation intensity	Area of correlation spot	I_p/N_{rms}	η_h	Peak correlation intensity	Area of correlation spot	I_p/N_{rms}	η_h
Tank vs. tank filter	1.95	836	326	6.38×10^{-3}	4.65	105	203	8.62×10^{-3}
Tank vs. truck filter	1.08	1519	208	1.54×10^{-2}	3.90	30	183	2.14×10^{-3}
Truck vs. tank filter	2.15	648	449	6.37×10^{-3}	6.24	77	270	5.13×10^{-3}
Truck vs. truck filter	1.55	714	409	4.91×10^{-3}	3.3	135	205	1.05×10^{-2}

Table 6. Comparative Correlation Results

	Amplitude and Phase (standard) FK filter				Phase-only FK filter			
Input	Peak correlation intensity	Area of correlation spot	I_p/N_{rms}	η_h	Peak correlation intensity	Area of correlation spot	I_p/N_{rms}	η_h
Tank vs. tank f lter	1.484	540	288	3.16×10^{-3}	9.99	45	663	3.03×10^{-3}
Tank vs. truck filter	3.01×10^{-2}	2666	10.3	4.41×10^{-2}	0.796	371	20.4	2.72×10^{-2}
Truck vs. tank filter	6.76×10^{-3}	7433	1.77	4.10×10^{-2}	0.486	378	31.56	2.30×10^{-2}
Truck vs. truck filter	1.70	20	461	3.82×10^{-4}	7.89	36	201.4	4.32×10^{-3}

Table 7.

Comparison of results for the BER algorithm obtained from a theoretical description of the algorithm and from a computer simulation of a hybrid (electronic/optical) implementation of the algorithm. The initial input was a constant intensity two-dimensional image; relative operator error (25%) was constant over the input image domain. Experimentally realizable results will be limited by the accuracy of the electronic processor.

	n-bit accuracy	
iteration	theoretical	simulation
0	2	2
1	4	4
2	6	6
3	8	8
4	10	10
5	12	12
6	14	14
7	16	16
8	18	18
9	20	20

Table 8.

Results from a computer simulation of a hybrid (electronic/optical) implementation of the BER algorithm using a sinusoidal input image function and a sinusoidal relative operator error function (max 25%).

	n-bit accuracy
iteration	simulation
0	2.0
1	4.0
2	6.0
3	8.0
4	10.0
5	12.0
6	14.0
7	16.0
8	18.0
9	19.9

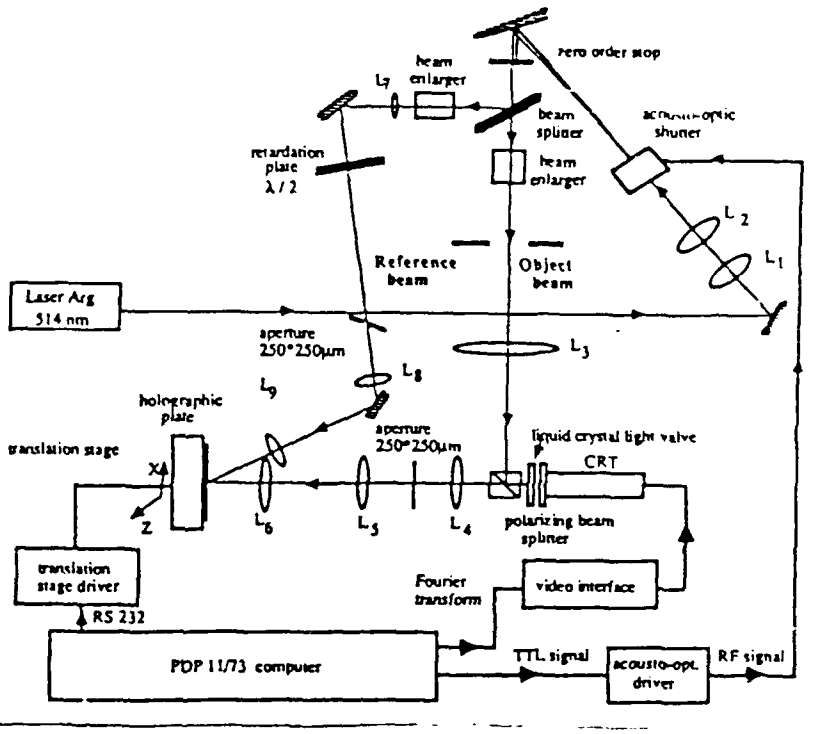

Fig. 1. Schematic of the hybrid system for producing computer generated space-variant holographic filters. A matrix of 256 by 256 holograms of different PSF is recorded with this system. The following focal length (f) in mm and F-number (F#) lenses are employed $f_1 = 100$, $f_2 = 20$, $f_3 = 360$, $f_4 = 80$ of F# = 1.6, $f_5 = 80$ of F# = 1.6, $f_6 = 80$ of F# = 1.6, $f_7 = 20$, $f_8 = 120$, $f_9 = 120$.

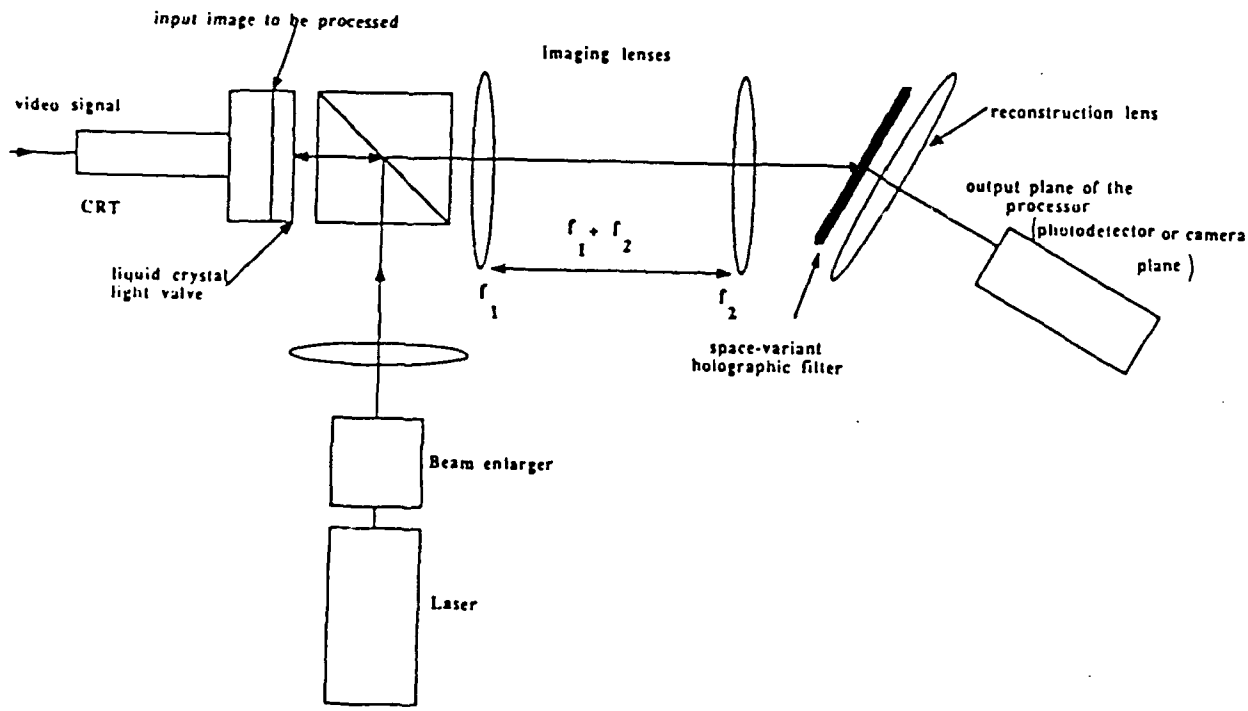

Fig. 2: Real time space-variant optical processor (Top view). The input pattern is displayed on the CRT/LCLV and imaged on the space-variant holographic filter. A camera is placed in the reconstruction plane of the holograms.

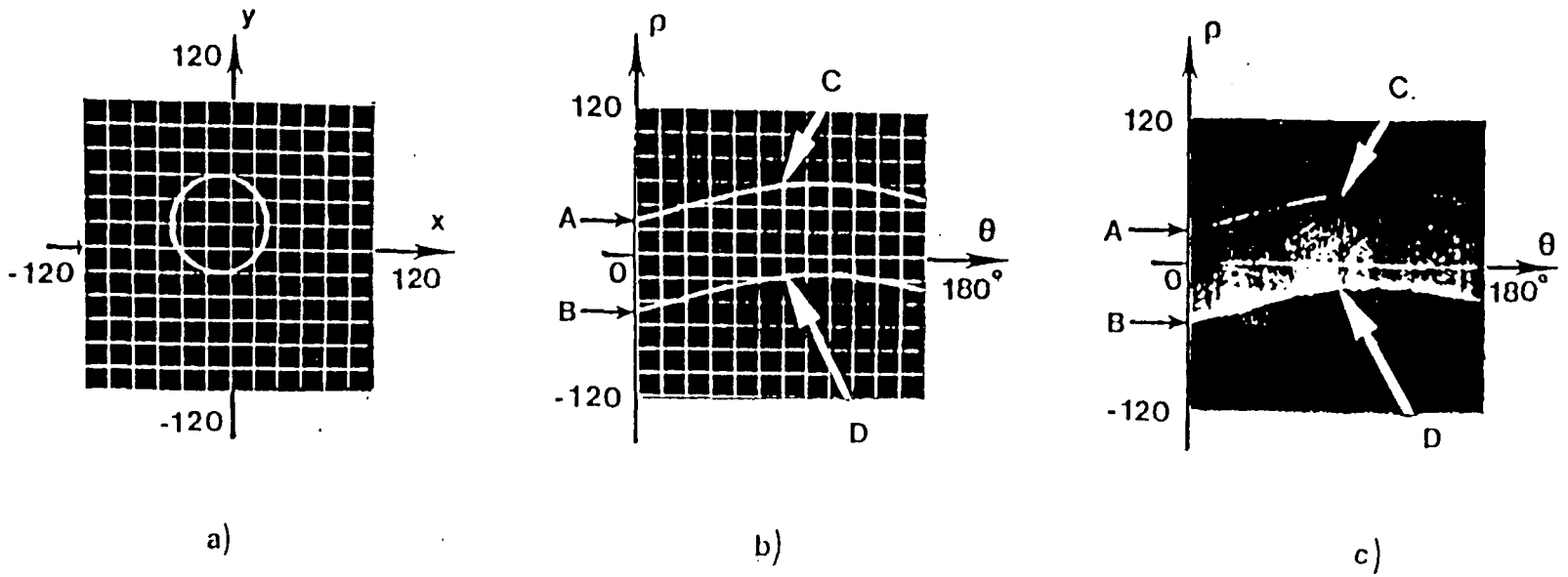

Fig. 3: Detection of the parameters of a circle with the HT. a) Input image of a circle of radius r = 40, centered at $(x_0, y_0) = (-10, 20)$. b) Computer calculation of the parameter domain. The parameters of the circle are determined from the coordinate of the points A, B, C and D. For A and B with coordinates (0, 30) and (0, -50) respectively the extracted parameters are r = 40 and $x_0 = -10$. For C and D with coordinates (90°, 60) and (90°, -20) the extracted parameters are r = 40 and $y_0 = 20$. c) Output of the optical processor from which the parameters r = 40, $x_0 = -10$ and $y_0 = 20$ can be extracted.

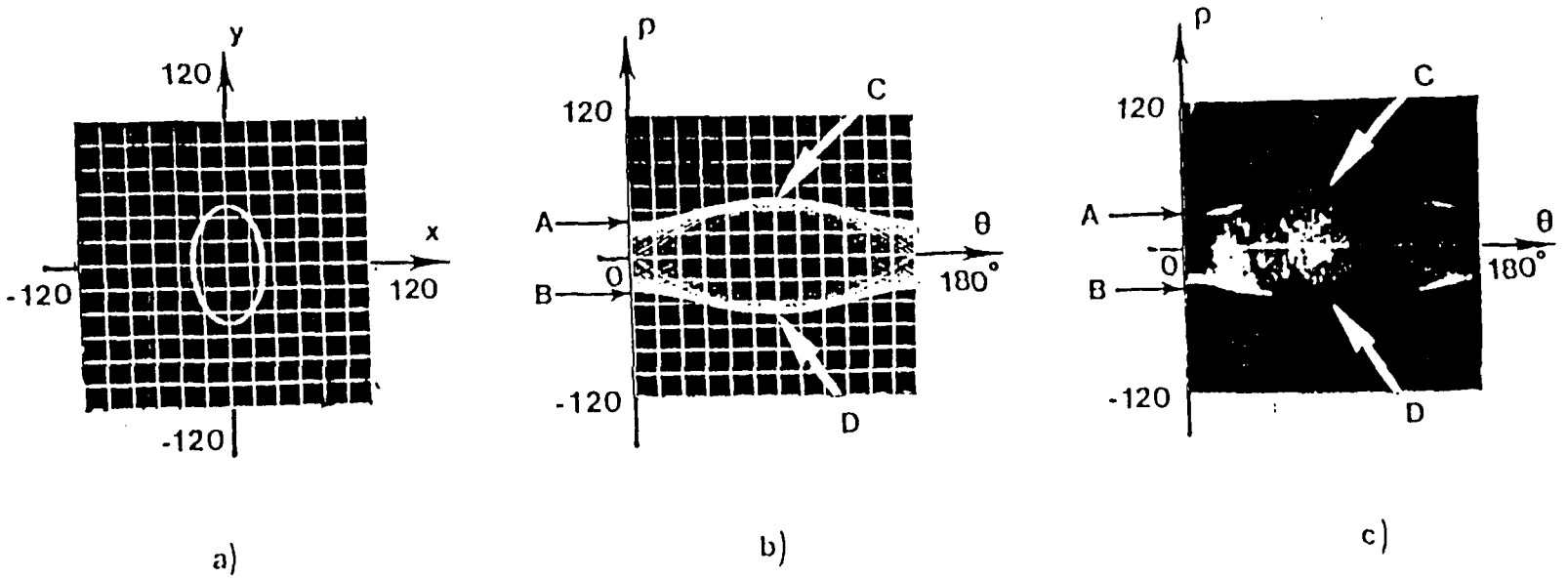

Fig. 4: Detection of the parameters of an ellipse with the HT. a) Input image of an ellipse centered at $(x_0, y_0) = (0, 0)$, and of axis a = 30 and b = 50. b) Computer calculation of the parameter domain. The parameters of the ellipse are determined from the coordinate of the points A, B, C and D. For A and B with coordinates (0, +30), and (0, 30) respectively the extracted parameters are a = 30 and $x_0 = 0$. For C and D with coordinates (90, 50), and (90, -50) the extracted parameters are b = 50 and $y_0 = 0$. c) Output of the optical processor for the same input ellipse from which the following parameters a = 30, b = 50, $x_0 = 0$ and $y_0 = 0$ can also be extracted.

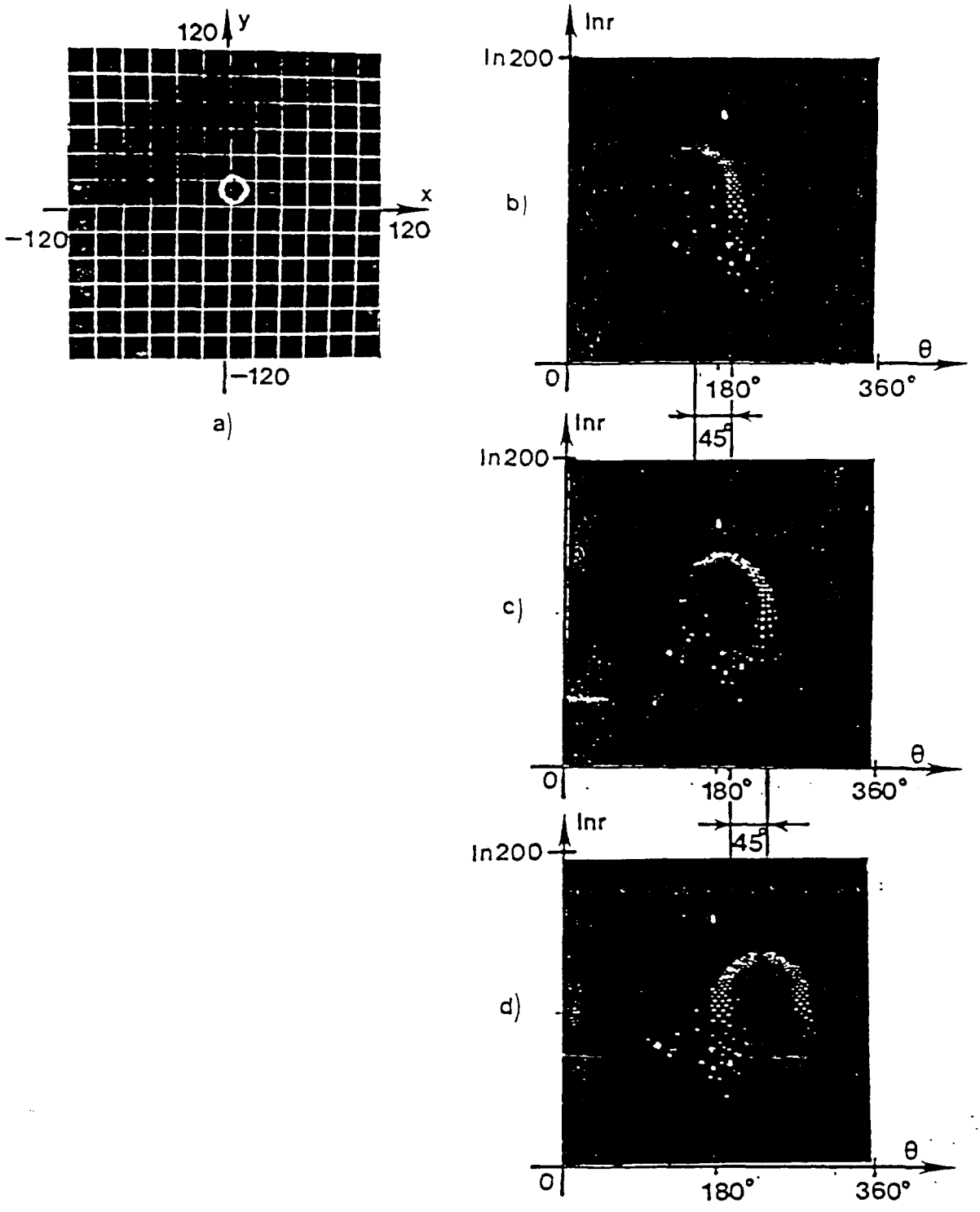

Fig. 5. $\ell n\, r-\theta$ coordinate transform of a rotation variant pattern. a) Original input image of an off-center circle. b) Optical coordinate transform $\ell n\, r-\theta$ of the input pattern. c) Optical coordinate transform of the input pattern rotated by an angle of 45° around the origin of the coordinate system. d) Optical coordinate transform of the input pattern rotated by an angle of 90° around the origin of the coordinate system.

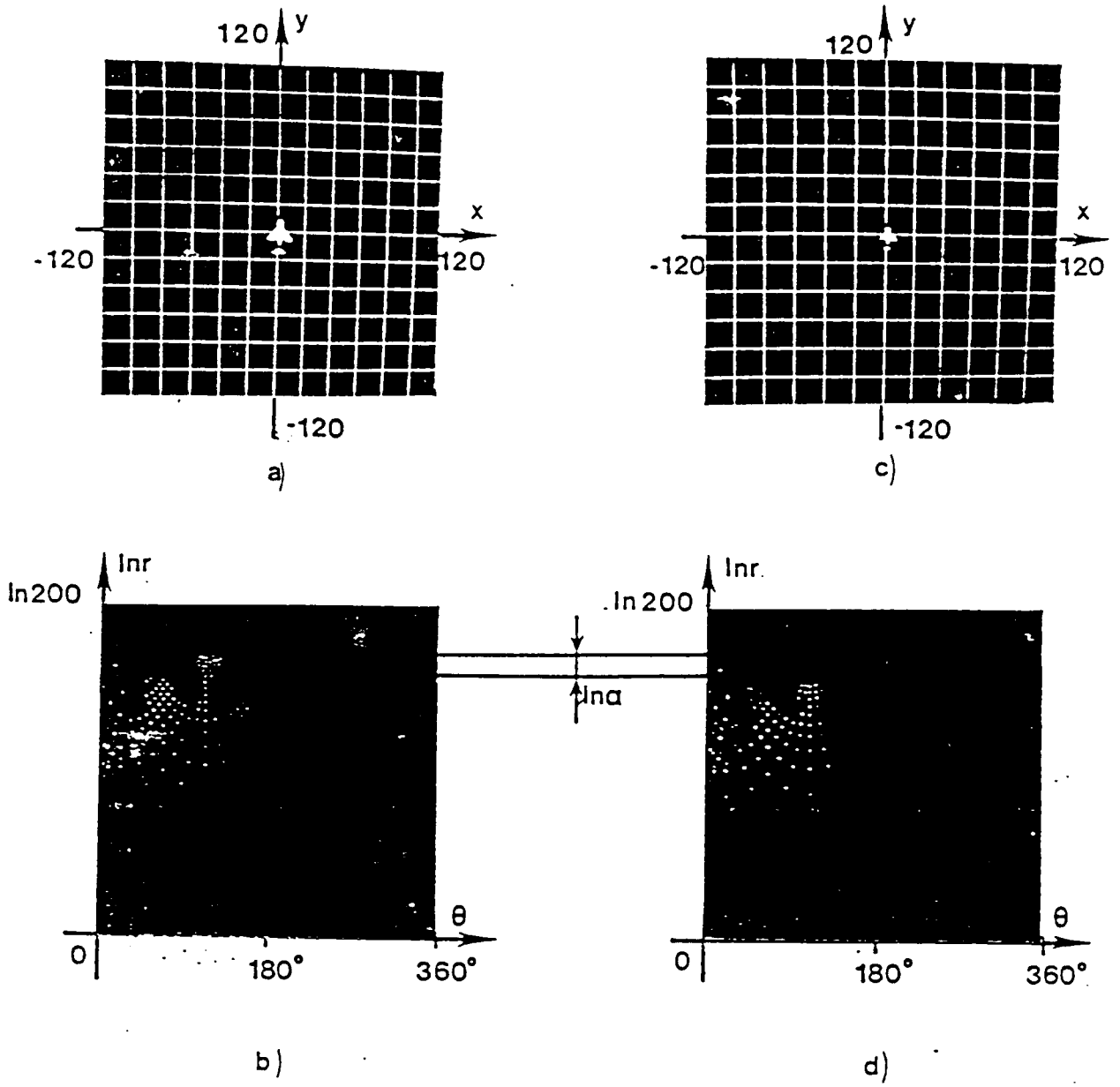

Fig. 6. $\ell n\, r - \theta$ coordinate transform of another scale variant pattern. a) Input image of an airplane, with original scale 1. b) Optical coordinate transform of the image in (a). c) Input image of (a) scaled by a factor of $\alpha = 0.7$. d) Optical coordinate transform of the image in (c). The transformed pattern of (b) is shifted upward by an amount of $\ell n\, \alpha$.

(a)

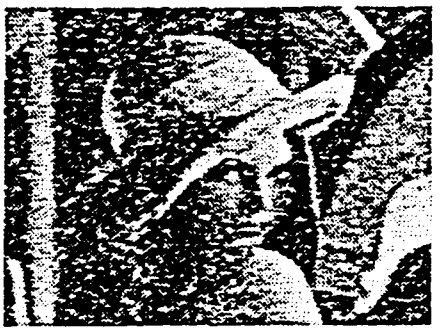

(b)

(c)

(d)

Fig. 7. (a) Original noisy image, (b) output of a low-pass filter, (c) output of a median filter, (d) output of the proposed space-variant filter.

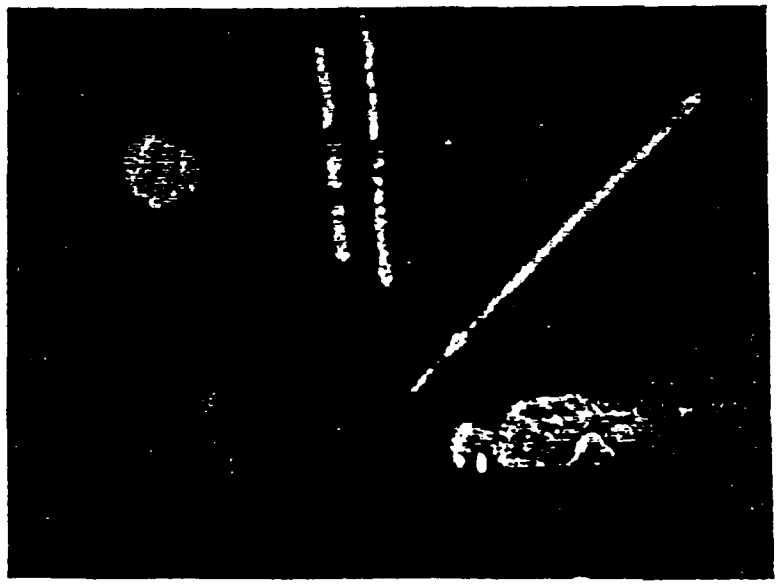

Fig. 8a. The transmitted output signal just after initial illumination of the stationary input scene. After a few seconds, the output vanishes completely. Notice the model car in the lower right.

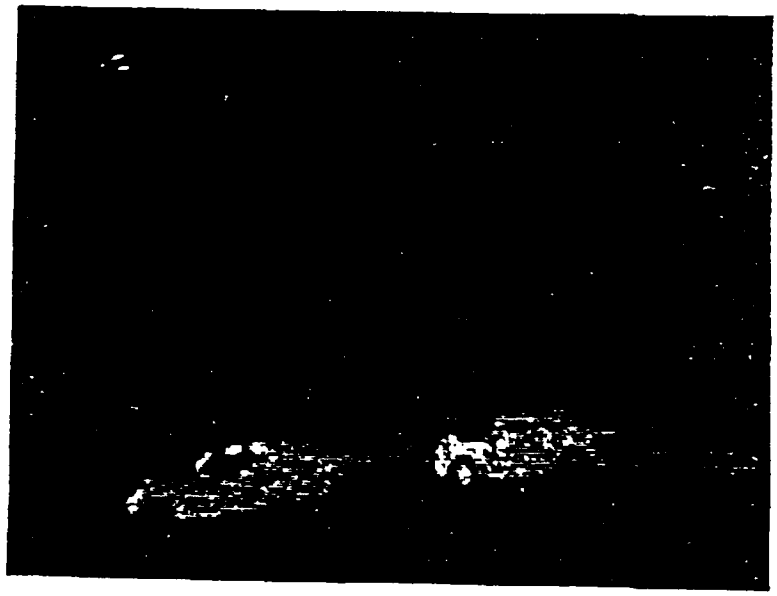

Fig. 8b. The transmitted output just after the model car was moved to the left. The car's initial and current positions are revealed, along with a fading trail of the most recent positions. The stationary components of the scene remain dark.

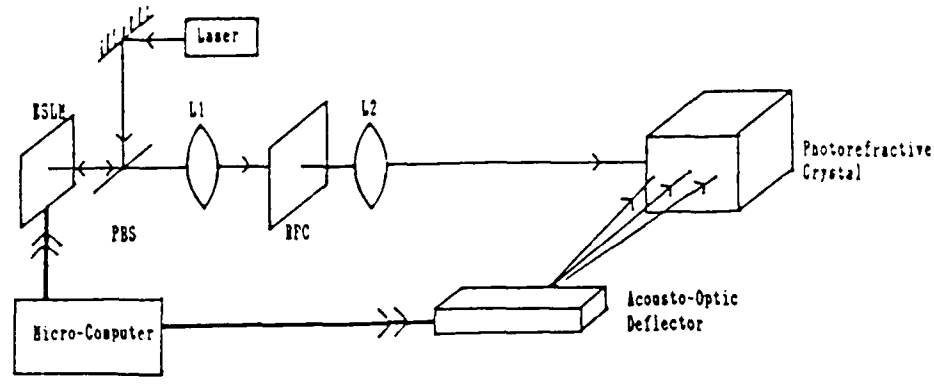

(a)

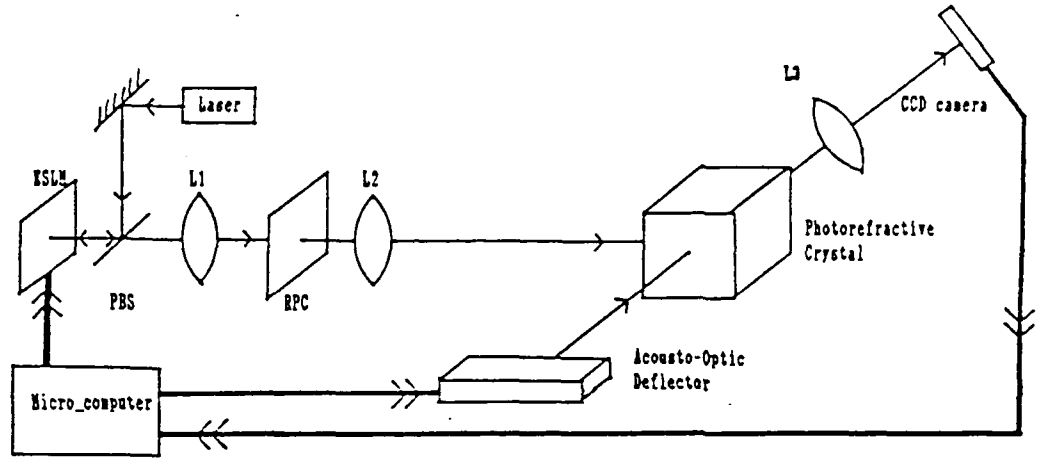

(b)

Fig. 9. (a) Tensor storage. The lmth component of W(l,m,y,y) tensor is displayed on the electronically addressed spatial light modulator (ESLM). Lense L1 images W(l,m,x,y) onto the random phase function $\exp[j\phi(x,y)]$. This random phase function is provided by a high resolution E-Beam fabricated random phase code transparency (RPC). The resulting product is Fourier transformed via lens L2 onto the photorefractive crystal while a reference plane wave, deflected by an angle la and ma, arrives from the acousto-optic device. The superposition of the first beam and the shifted reference beam creates the appropriate interference hologram. The space bandwidth product of the photorefractive crystal is high (10^9) and will allow the storage of a large W(l,m,x,y) tensor. (b) Random Phase Coded Matrix Tensor Multiplication: When G(x,y) is presented during readout, the lm correlations of W(l,m,x,y) with G(x,y) sharpened by the random phase function are transmitted along the various (la,ma) directions. This beam is then Fourier transformed by lense L3 and captured by the CCD camera.

After the initial inputs to W(l,m,x,y) are made the two phases of operation will alternate. An image will be input and the correlations determined. Then the appropriate lmth component of W will be updated by an amount determined by the algorithm. The alternation of these two phases provides the system with the ability to adjust the weighting factors and to learn new categorizations as they appear.

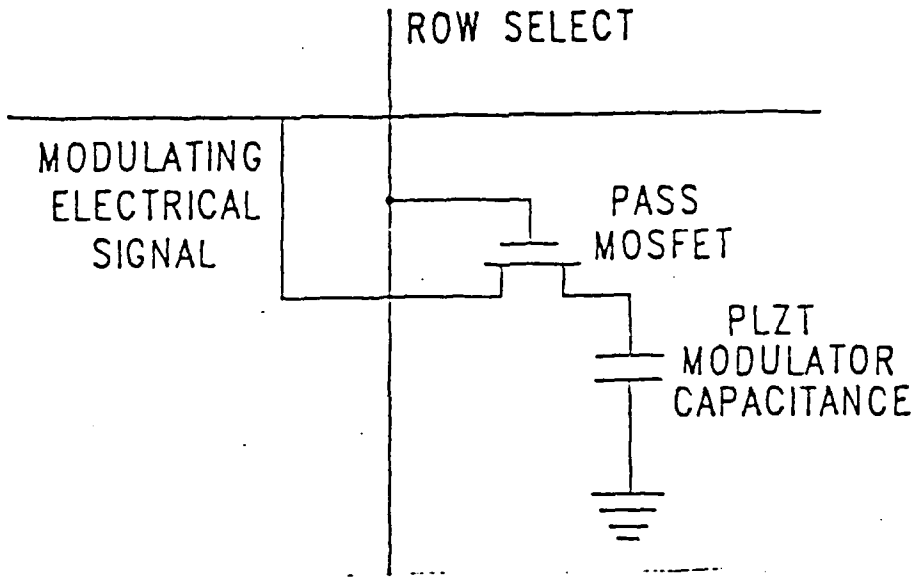

Fig. 10a. Schematic of the ESLM circuit in each unit cell.

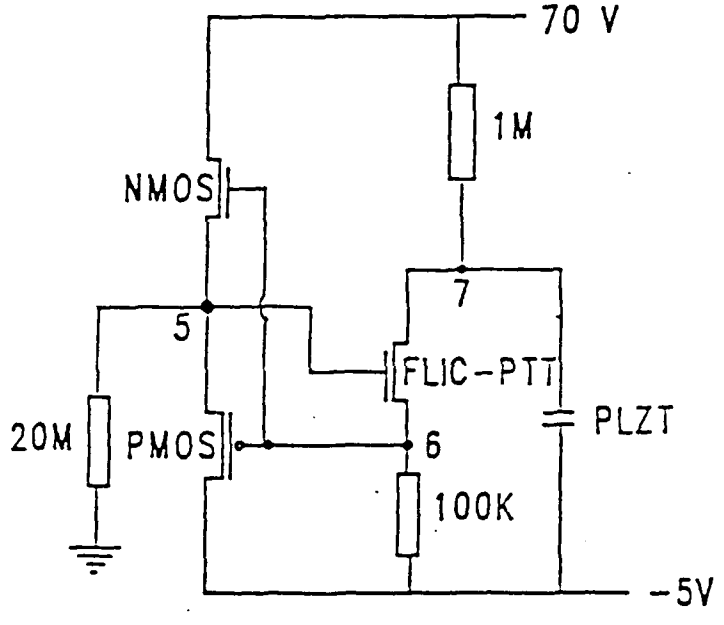

Fig. 10b. Schematic of the fabricated OSLM circuit in each unit cell.

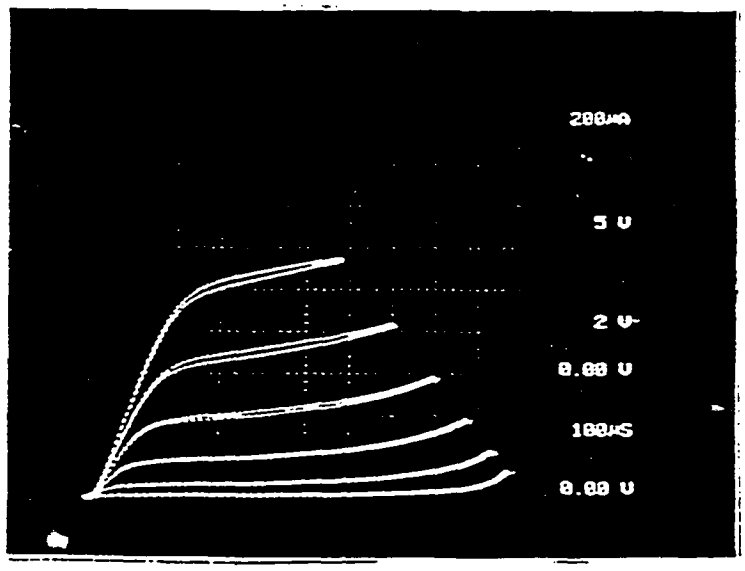

Fig. 11a. I-V characteristics of a typical NMOS pass transistor used in the ESLM circuit.

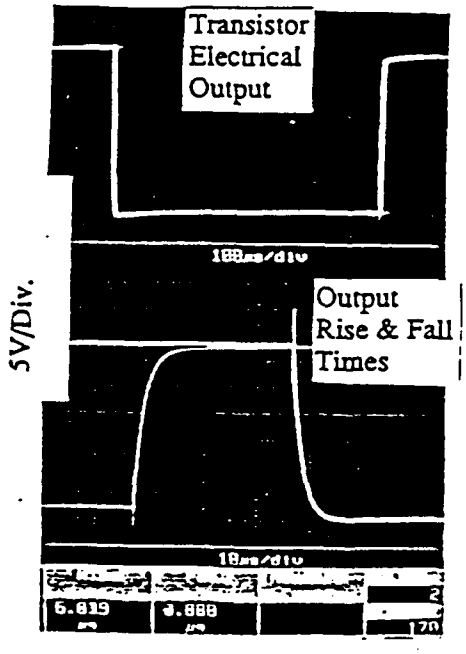

Fig. 11b. Response time characteristics of ESLM. The upper curve is plotted on a longer time scale. the lower curve shows the rise and fall times in detail on a shorter time scale.

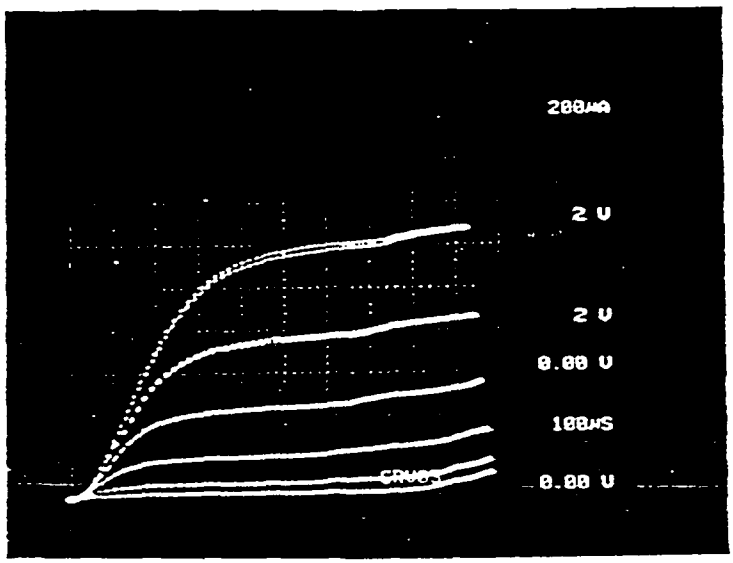

Fig. 12 Typical I-V characteristics of Si/PLZT NMOS transistor utilized in OSLM array.

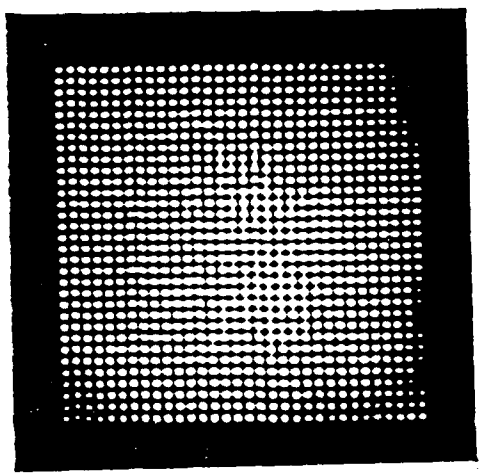

Fig. 13. Optical reconstruction from one of the 32 × 32 arrays of holograms for full interconnection among the 32 × 32 processing elements.

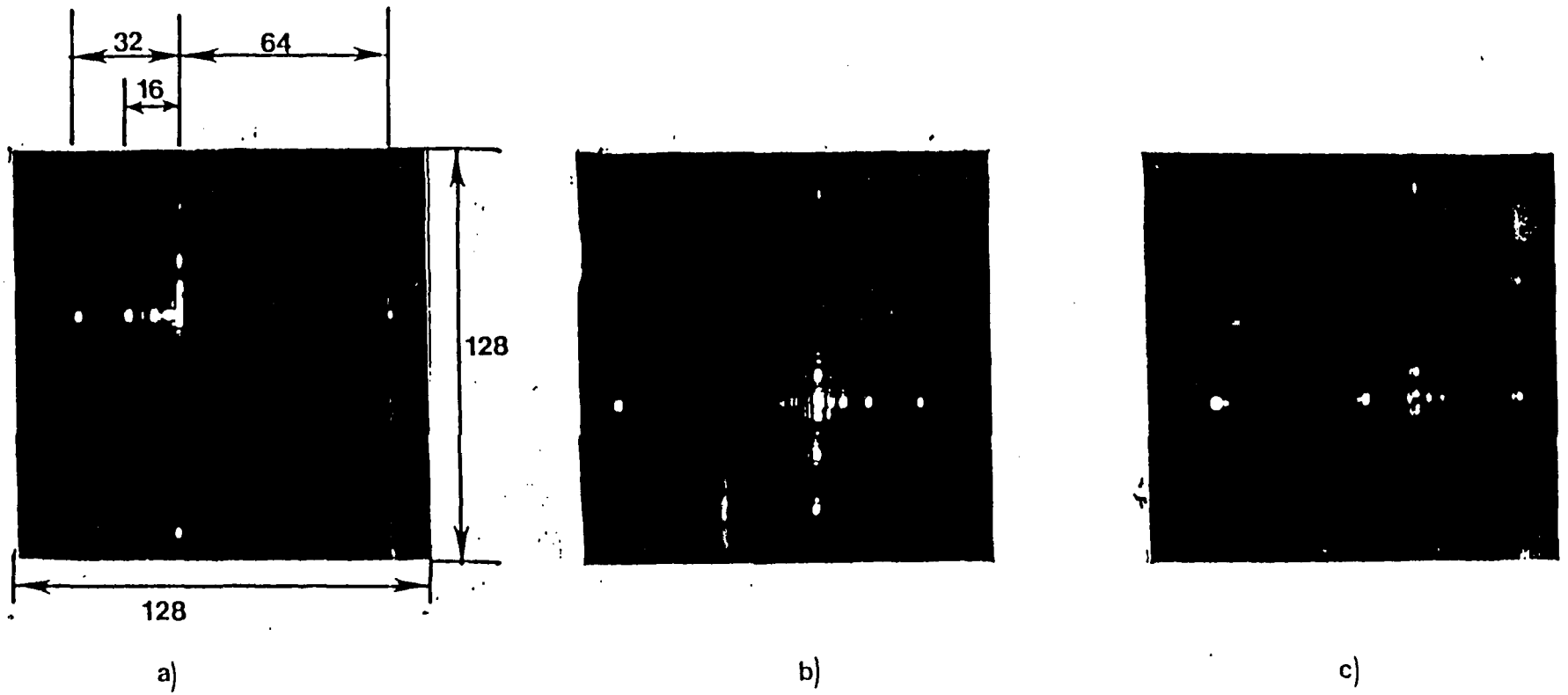

Fig. 14. Reconstruction of the HOE for hypercube interconnect 128 × 128 PE's. (a), (b) and (c) show three examples of the connection pattern for three different nodes of the PE array and are obtained by illuminating the holograms corresponding to these PEs. The $\log_2 128 = 7$ visible spots in each direction show the connection from one PE to seven PEs in each direction.